Available online at www.sciencedirect.com
SCIENCE DIRECT
ELSEVIER
Journal of Magnetism and Magnetic Materials 283 (2004) 335–343
Journal of magnetism and magnetic materials
www.elsevier.com/locate/jmmm

Magnetorheological suspension based on mineral oil, iron and graphite micro-particles

Ioan Bica

Department of Physics, Faculty of Physics, West University of Timisoara, Bd. V. Parvan, no. 4, 1900 Timisoara, Romania

Received 24 March 2004; received in revised form 9 April 2004
Available online 26 June 2004

Abstract

The paper presents the process of obtaining magnetorheological suspensions based on mineral oil, iron and graphite micro-particles and thermal decomposition of $Fe_2(CO)_9$. The suspension is characterized by its magnetic and magnetorheological properties. The device presented in the paper is used to determine the electrical conductivity of the suspension under the influence of the magnetic field and to interpret the results obtained in this manner.

PACS: 75.50.T

Keywords: Magnetorheological suspensions; Graphite; Iron micro-particles; Magnetic field; Electrical conductivity

1. Introduction

Magnetorheological suspensions (MRS) are polyphase fluids. They comprise a liquid (silicon oil, mineral oil, etc), the stearic acid and magnetic micro-particles [1–3]. The orientation of the latter ones follows the lines of the external magnetic field. The strength of the particle chains depends on the intensity of the magnetic field, the dimension of the particles, the concentration of the suspensions, and on the magnetic properties of the micro-particles [4–12].

Sensible manifestations of the viscosity of the suspension in magnetic field. For suitable values of the intensity of the magnetic field, the suspension Bingham plastic [11–15]. These properties of MRS are successfully used in the following areas:

- dampers for the attenuation of vibrations [16–20] and absorption of seismic shocks [20–22];
- under the influence of brakes and clutches with pre-established coupling coefficients an external magnetic field [16,23,24];
- manufacturing of orthopedic protheses [24,25] and, last but not least, in bio-medical studies [26].

E-mail address: ibica2@yahoo.com (I. Bica).

0304-8853/$ - see front matter
doi:10.1016/j.jmmm.2004.05.036

The manufacturing of sensors or/and magnetic field transductors, as well as resistors with resistance values controlled by an external magnetic field, is based on the production of MRS electroconductors [27].

2. Experimental device for the production of MRS

The illustrative scheme of the device for the production of MRS is shown in Fig. 1. In this figure, the description and main technical characteristics of the installation comes from Ref. [3].

The liquid matrix (location 8 in Fig. 1) has the structure presented in Table 1. The thermal treatment of the matrix is achieved according to the temperature–time diagram displayed in Fig. 2.

During thermal treatment, the oil in the liquid matrix was supplemented with mineral oil, originating from the basin *F*, in quantities with up to 18.5×10^{-3} kg.

One-chamber ($60 \times 10^{-6}\,\mathrm{m}^3$), 2-pipe for argon dispersion, 3-palette, 4-oil supplying, 5-thermocouple iron-constantan, 6-autotransformer (0–220 $V_{ac}/8A_{ac}$), 7-heater (500W), 8-liquid matrix, "*a*"and "*b*"-electric outlets (220 V_{ac}).The water input and the water output are displayed by the arrow sequence "—— →"and "→ →", respectively.

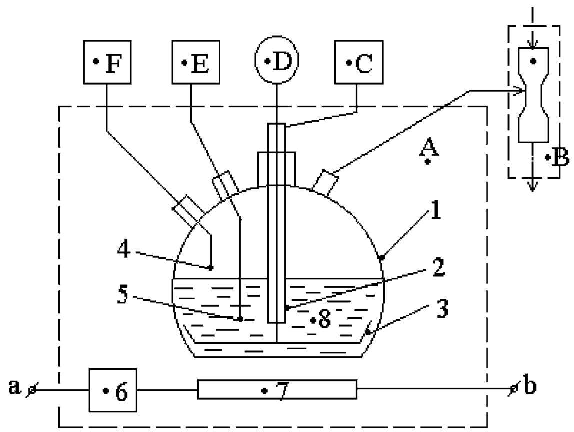

Fig. 1. The illustrative scheme of the experimental device designed to produce magnetorheological suspensions: (A) chemical reactor; (B) water ejector vacuum pump; (C) the gas container, (D) electric motor ($24\,V_{dc}/3A_{dc}$; 0–50 rev s^{-1}), (E) indicator millivoltmeter, (F) mineral oil supplier.

Table 1
The structure of the liquid matrix

$10^3 \times m_1$ (kg)	$10^3 \times m_2$ (kg)	$10^3 \times m_3$ (kg)	Obs.
25	82	1.5	—

Note: m_1: the mineral oil mass (ANERON-Merck type), m_2: the $Fe_2(CO)_9$ mass (powder of granulation ranging between 4.5 and 5.2 μm, with a minimum of 97% Fe), m_3: the stearic acid mass.

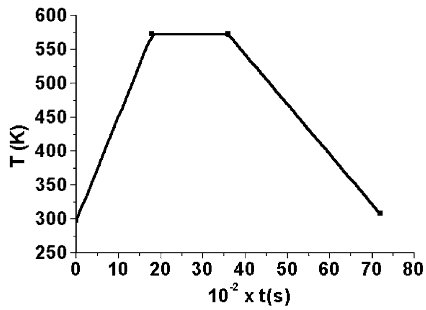

Fig. 2. Temperature–time diagram.

The argon flow, injected from the cylinder C through the tube 2 (Fig. 1) into the liquid matrix, is of 5 l min^{-1} ($83.33 \times 10^{-6}\,\mathrm{m}^3\,\mathrm{s}^{-1}$). The pressure in the enclosure 1 is maintained at –220 mm.col. $H_2O \pm 10\%$ ($-2.0594\,\mathrm{Pa} \pm 10\%$). $Fe_2(CO)_9$ is heated up to $T = (573 \pm 10\%)$ K (Fig. 2) during 30 min (1.800 s) and it decomposes thermically.

Starting from 573 K, the liquid matrix 8 (Fig. 1) is cooled at the velocity of $0.074\,\mathrm{K\,s}^{-1}$, to $(314 \pm 10\%)$ K. Whenever the stearic acid mass is larger than 1.5×10^{-3} kg, the liquid matrix gets transformed into a plastic body.

The shape and the dimensions of the particles in the suspension are shown in Fig. 3a, while the dimensional distribution of the particles is displayed in Fig. 3b.

The mean diameter of the iron particles is 0.595 μm, with a standard deviation of 0.337 μm.

The iron particles are not oxidated and do not get oxidated during time. This is due to the underlying production procedure as well as the fact that an oil layer with stearic acid as well is adsorbed on the surface of the particles [28].

At the temperature of $(314 \pm 10\%)$ K of matrix 8 in room 1 (Fig. 1), one introduces graphite in

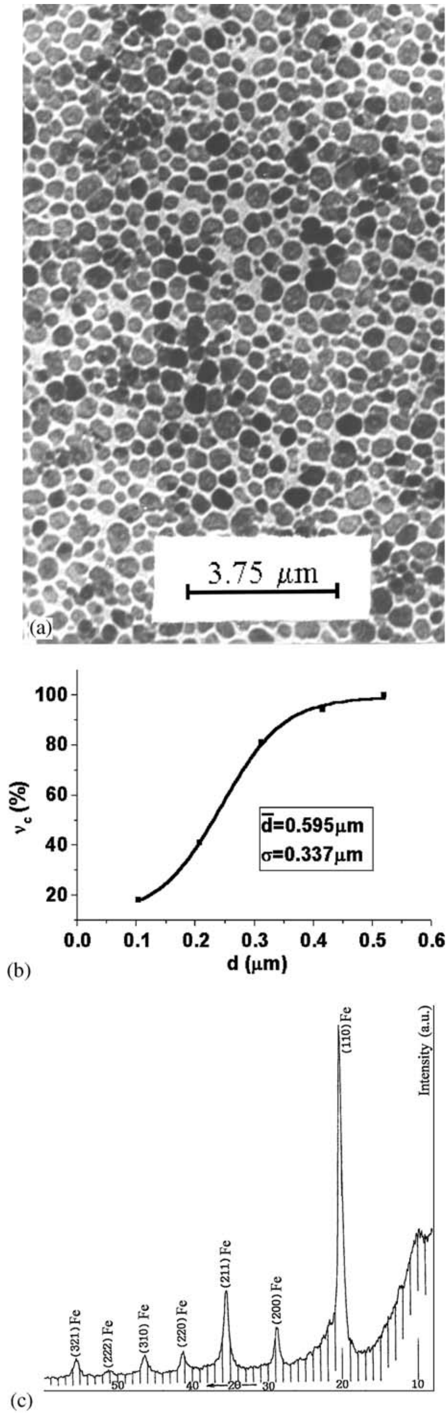

Fig. 3. The iron micro-particles: (a) shapes and dimensions, (b) dimensional distribution (v_c is the cumulated frequency, d is the particle diameter, $\bar{d}$ denotes the mean particle diameter and σ is the standard deviation), and (c) röentgenogram.

Table 2
The compositions of EMRS

$10^3 \times m_1$ (kg)	$10^3 \times m_2$ (kg)	$10^3 \times m_3$ (kg)	$10^3 \times m_4$ (kg)	Obs.
25	25.23	1.5	6.21	—

Note: m_1: the mineral oil mass (ANERON-Merck type), m_2: the mass of the iron particles (of mean diameter 0.595 µm at a standard deviation of 0.337 µm), m_3: is the stearic acid mass, and m_4: the mass of the graphite powder.

powder form (its granulation ranging between 2 and 32 µm) whereas the mechanical mixing is performed with the palette 3 (10 rev./s ± 10%).

Proceeding in this manner, a magnetorheological suspension based on mineral oil, iron micro-particles and mineral oil (EMRS) is formed. The composition of EMRS is presented in Table 2.

The EMRS in a 1:1000 dilution with mineral oil visualized by the optic microscope is presented in Fig. 4.

The MRS magnetization curve and the EMRS magnetization curve are presented in Fig. 5. For this purpose a magnetometer with a vibratory specimen (VSM 880 type) has been used.

It can be seen from Fig. 5 that the saturation magnetization of EMRS is about 7% lower than the saturation magnetization curve of MRS. This difference is due to the influence of graphite in the EMRS composition (Table 2).

The magnetorheological characterization of the suspensions is presented in Fig. 6 for values of H, at which the magnetization of the suspensions exhibits the same values.

For these measurements, a magneto-rheological device (type Physica MRC 300), has been used.

The increased values for the dynamic viscosity η and the shear stress τ of EMRS as compared to the ones of MRS, are due to the form of the graphite micro-particles [29].

3. Electrical conductivity

3.1. Experimental device

The experimental device used for the determination of the electrical conductivity of the

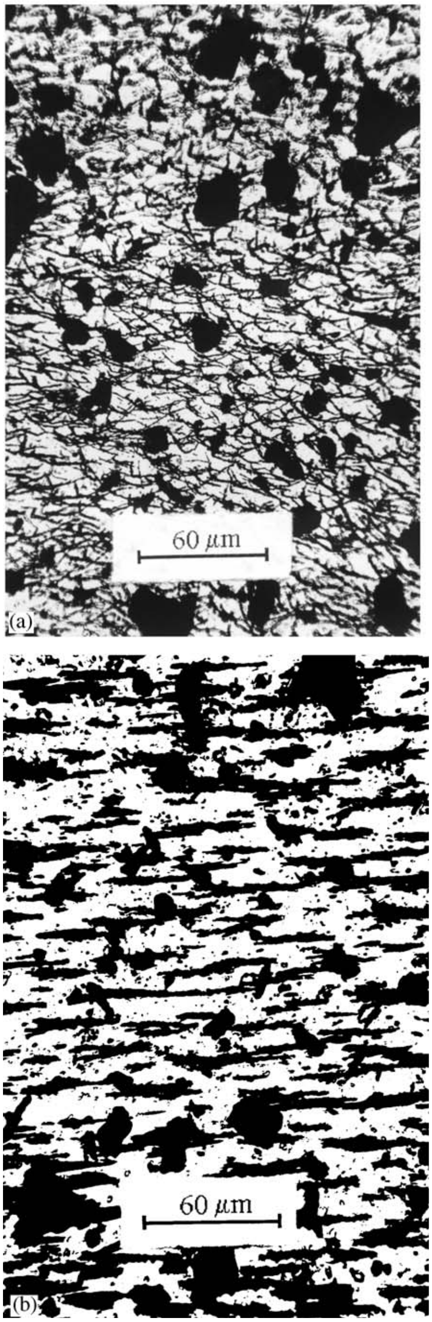

Fig. 4. The MRS graphite mixture: (a) in the absence of the external magnetic field and (b) in the presence of the external magnetic field.

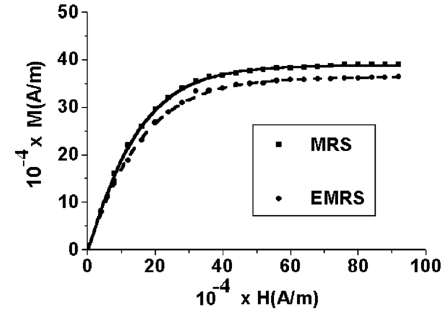

Fig. 5. The magnetization M of the MRS and the magnetization M of the EMRS versus the intensity H of the magnetic field.

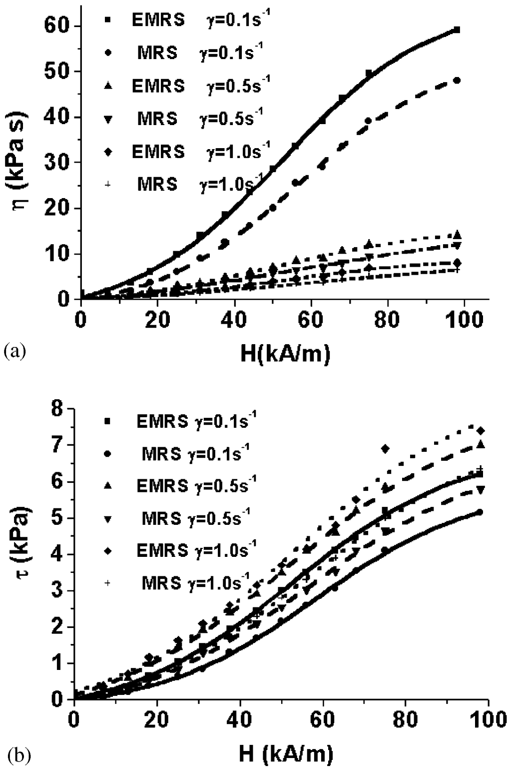

Fig. 6. Magnetorheological data. (a) the variation of the dynamic viscosity η as a function of the intensity H of the magnetic field and (b) the variation of the shear stress as a function of the intensity H of the magnetic field. In both cases, the $\dot{\gamma}$'s stand for parameters.

suspensions is shown in Fig. 7. It consists of an electromagnet (1), the measure cell (2), the ohmeter (3), (Voltcraft VC 332 type), the teslameter (4), (GM04, Hirst type) with the Hall sonde (5) and the steady current source S with the ampermeter A (Voltcraft M-3650B type).

The detailed design of the electromagnet from position 1 in Fig. 7 is presented in Fig. 8. The electromagnet has attached screws (position 3 in Fig. 8). They serve for fixing of the polar parts of measuring cells on the electromagnet.

The detailed configurations of the measure cells are presented in Figs. 9 and 10. The dependence of the intensity H of the magnetic field such as measured at point O (Figs. 9 and 10), on the intensity I of the current through the coil of the electromagnet is displayed in Fig. 11a. The values of the magnetic field intensity gradient in the space between the polar parts as a function of the intensity of the current through the coil of the electromagnet are presented in Fig. 11b.

The modulus dH/dx of the gradient of the magnetic field as a function of the intensity I of the current. (A) longitudinal magnetic field. (B) transversal magnetic field.

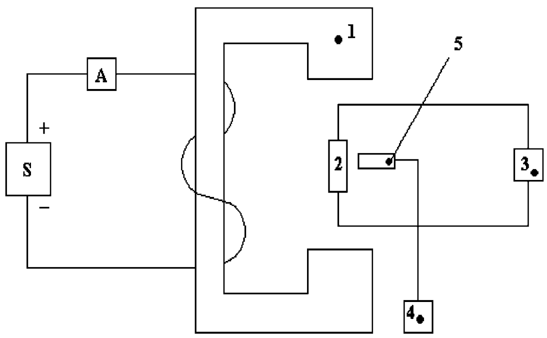

Fig. 7. Experimental device for determining the electrical conductivity σ of the magnetorheological suspensions (block scheme): 1—electromagnet, 2—measuring cell, 3—ohmmeter, 4—teslameter, 5—Hall probe, A—ampermeter, S—current supply.

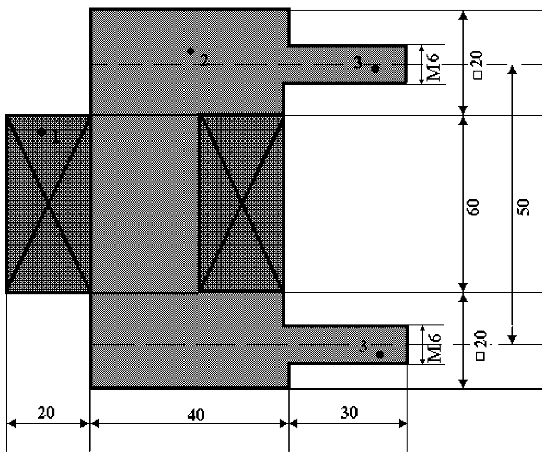

Fig. 8. Electromagnet (overall configuration): 1—coil, 2—core, 3—screws.

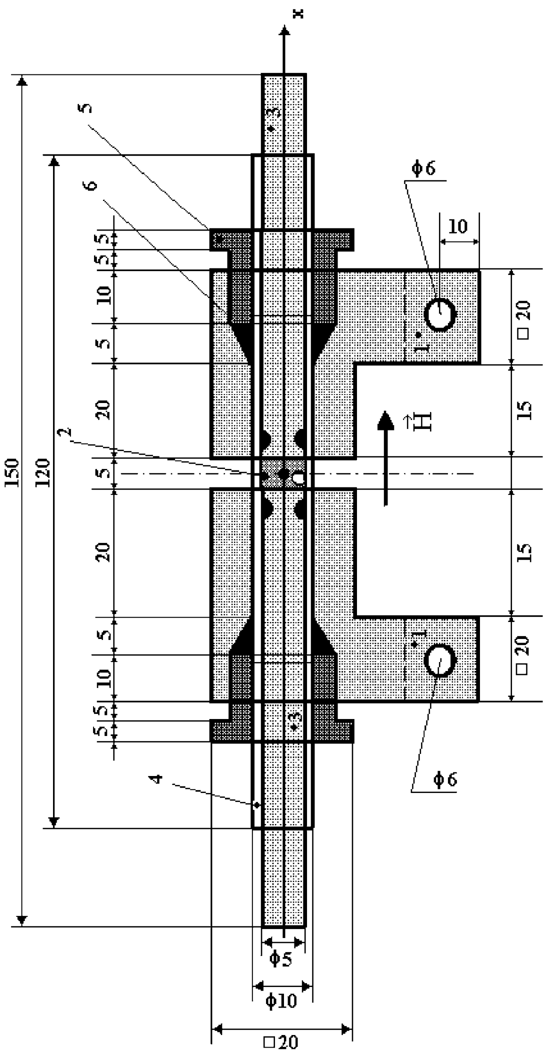

Fig. 9. Overall configuration of the measuring cell for the case in which the applied magnetic field is parallel to the specimen. 1—magnetic pole, 2—specimen (suspension), 3—electrode (non-magnetic), 4—glass cylinder, 5—nut, 6—rubber fitting.

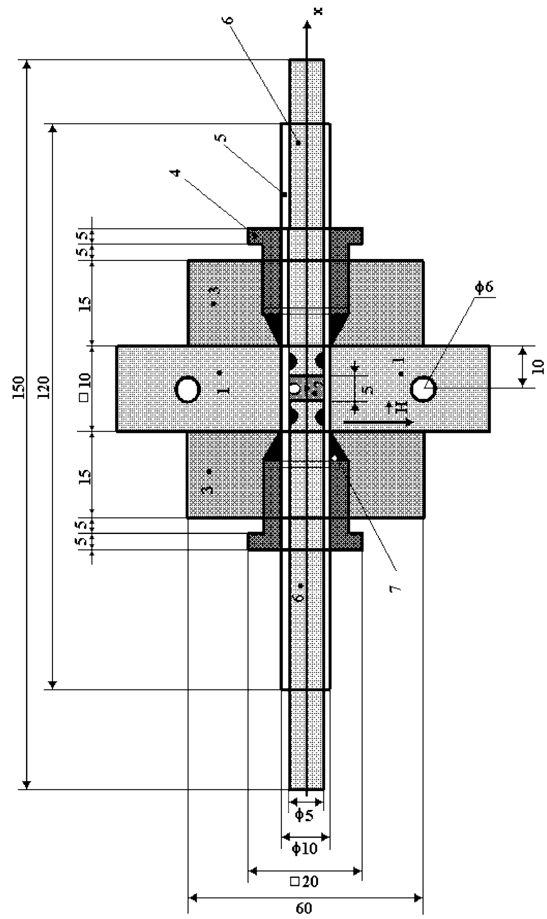

Fig. 10. Measuring cell for the case in which the magnetic field is applied perpendicularly to the specimen. 1—magnetic pole, 2—specimen (suspension), 3—fixing element (non-magnetic), 4—nut, 5—glass cylinder, 6—electrode (non-magnetic), 7—rubber fitting.

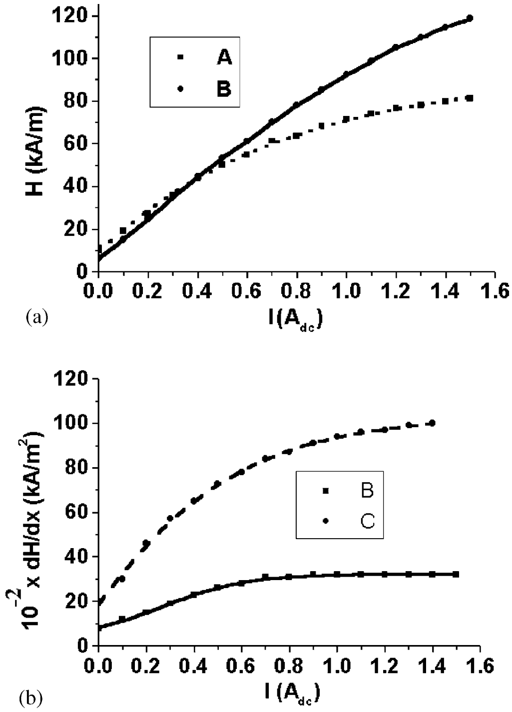

Fig. 11. The intensity H of the magnetic field as a function of the intensity I of current (a) $\mathrm{d}H/\mathrm{d}x$ as a function of the intensity I of the current (b). (A) longitudinal magnetic field, (B) transversal magnetic field.

3.2. Experimental results and discussion

The length of the suspensions (position 2 in Figs. 9 and 10) is equal to their diameter, that is 5×10^{-3} m. The measurement of the resistance R of the suspension specimen is achieved by means of the experimental device presented in Fig. 7. The resistance R of the suspension is the one measured at the moment of the application of the magnetic field. Other values of R are recorded at interval of 15 s.

From values and dimensions of the specimen, the electrical conductivity of the suspension is determined via

$$\sigma\,(\mho) = \frac{250}{R(M\Omega)}. \tag{1}$$

The temperature of the suspension is $(297 \pm 5\%)$ K. The MRS exhibiting the composition shown in Table 1 is a magneto-dielectric one. On the other hand, the suspension having the composition shown in Table 2 concern a conducting phase. Values of the electrical conductivity σ of EMRS are shown in Fig. 12. The magnetic pressure generated in the suspension by the magnetic field is [15]:

$$\Delta p_{\mathrm{magn}} = \mu_0 M_{\mathrm{s}} H h / 2r, \tag{2}$$

in which μ_0 is the magnetic permeability of the vacuum, M_{s} is the saturation magnetization of the suspension, whereas h and $2r$ are the length and the diameter of the specimen, respectively.

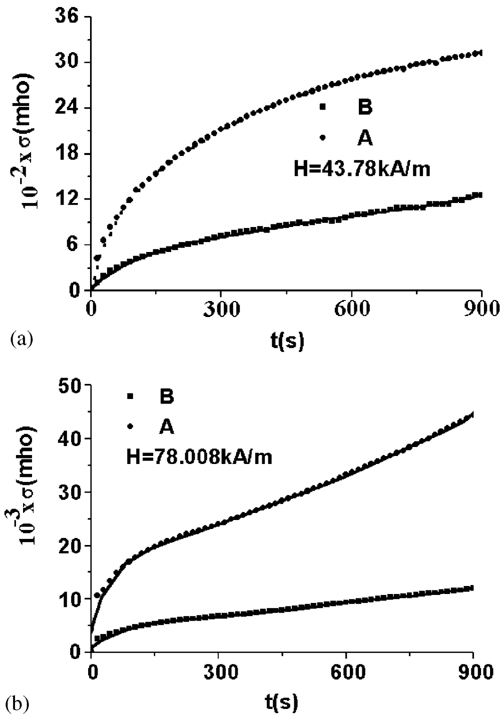

Fig. 12. The variation of the conductivity σ of EMRS during the application of the magnetic field, for: $H = 43.780\,\mathrm{kA/m}$ (a) and $H = 78.008\,\mathrm{kA/m}$ (b). (A) longitudinal magnetic field, (B) transversal magnetic field.

The magnetic particles follow, of course, the magnetic field lines. When the magnetic field is applied parallel to the suspension specimen, the contact resistance between the electrodes of the device in Fig. 7 is much smaller as compared to that when the magnetic field is perpendicular to the specimen, due to Δp_{magn}. Fig. 12 shows that, for a given t, the high values of σ obtained under conditions of which the magnetic field is parallel to the suspensions, are much larger than the ones corresponding to a transversal field. We have to account for magnetic field gradients, under the conditions for which the magnetic field is not uniform, as indicated in Fig. 11b. Then, graphite particles, driven by the magnetic ones, migrate in the direction of the magnetic field gradient [29]. Let us consider an easy configuration in which the field is applied along the "x"-axis. Then the motion of the particles is governed by the equation [29]

$$M\frac{\mathrm{d}^2x}{\mathrm{d}t^2} + \xi\frac{\mathrm{d}x}{\mathrm{d}t} + \mu_0\mu_r m\delta = 0, \tag{3}$$

where M is the mass of the magnetic micro-particle, ξ is the micro-particle friction coefficient, μ_r is the relative magnetic permeability of the suspension, m is the magnetic moment and $\delta = \mathrm{d}H/\mathrm{d}x$ is the value of the gradient of the magnetic field intensity.

Considering that at the initial moment ($t = 0$) the distance between particles is $x(0) = \Delta$ such that $x'(0) = 0$, one obtains [29]

$$x(t) = \Delta + \frac{\mu_0\mu_r m\delta M}{\xi^2}\left[1 - \exp\left(-\frac{\xi}{M}t\right) - \frac{\xi}{M}t\right] \tag{4}$$

If $t \gg (M/\xi) \approx 10^{28-}\,\mathrm{s}$ [29], one has $\exp(-(\xi/M)t) \to 0$, so that Eq. (4) becomes

$$x(t) = \Delta + \frac{\mu_0\mu_r m\delta M}{\xi^2}\left(1 - \frac{\xi}{M}t\right) \tag{5}$$

At this point we shall consider that particles meet together at the migration time, which amounts to saying that $x = 0$ when $t = t_{\mathrm{mig.}}$.

Accordingly, one obtained

$$t_{\mathrm{mig.}} \cong \frac{\Delta\cdot\xi}{\mu_0\mu_r m\cdot\delta} = \frac{3\pi\cdot\eta\cdot d}{\mu_0\mu_r m\cdot\delta}\Delta \tag{6}$$

by virtue of Eq. (5) where $d = 0.595\,\mu\mathrm{m}$ is the diameter of the magnetic particles in EMRS, $\xi = 10^{8-}\,\mathrm{kg/s}$ and $m \approx 10^{14-}\,\mathrm{A\,m^2}$.

It is seen from Fig. 5 that $\mu_{\mathrm{MRS}} \approx \mu_{\mathrm{EMRS}} = 3$ for $H < 100\,\mathrm{kA/m}$. From the viscosity measurements presented in Fig. 6, one obtains $\eta = 24$ and $50\,\mathrm{kPa\,s}$ for $H = 43.780$ and $H = 78.008\,\mathrm{kA/m}$, respectively.

So, the magnetic field gradients concerning Fig. 11b are given by $\delta = 66\,\mathrm{kA/m^2}$ ($H = 43.780$ kA/m) and $\delta = 98\,\mathrm{kA/m^2}$ ($H = 78.008\,\mathrm{kA/m}$) for a transversal magnetic field, while $\delta = 24\,\mathrm{kA/m^2}$ ($H = 43.780\,\mathrm{kA/m}$) and $\delta = 30\,\mathrm{kA/m^2}$ ($H = 78.008\,\mathrm{kA/m}$) for a longitudinal one.

Eq. (6) also furnished the Δ-dependence of the migration time, as shown in Fig. 13.

It follows from Fig. 13 that the distance Δ between the graphite particles is located between 0.01 and 0.1 nm. Under the action of the magnetic field pressure Δp_{magn}, at $t = t_{mig.}$, the inter-particle distance gets diminished, as indicated in Fig. 13. Accordingly, the contact resistance between the graphite particles and the electrodes (position 3 in Fig. 9 and position 6 in Fig. 10) diminishes itself and the conductivity σ increases with time as shown in Fig. 12. The same method was used to determine the field dependence of the conductivity as shown in Fig. 14. The value of σ was determined 15 s after the application of the magnetic field's intensity. The measurements were performed at intervals of 45 s.

One sees from Fig. 14 that σ depends on the value of the intensity of the magnetic field and it is considerably influenced by the direction of the field with respect to the specimen.

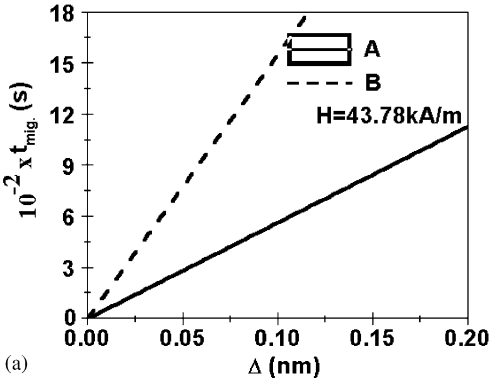

(a)

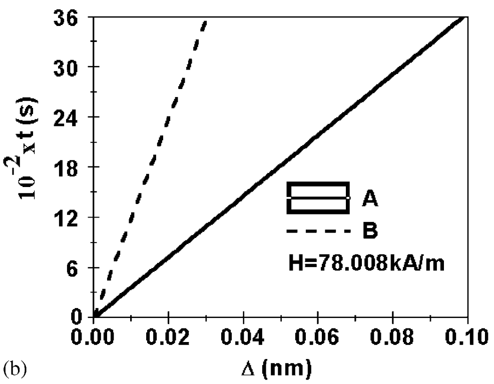

(b)

Fig. 13. The migration time $t_{mig.}$ of the suspension micro-particles as a function of the distance Δ between the micro-particles, for $H = 43.780$ kA/m (a) and $H = 78.008$ kA/m (b). (A) longitudinal magnetic field, (B) transversal magnetic field.

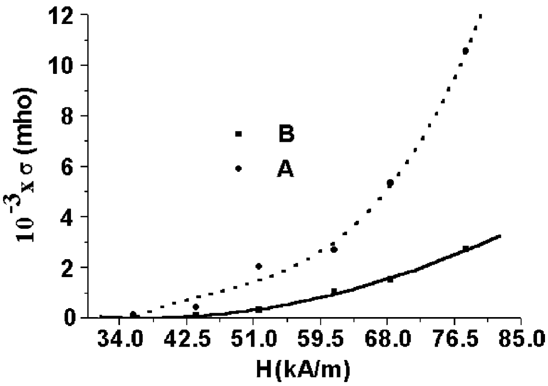

Fig. 14. The conductivity σ versus the intensity H of the magnetic field. (A) longitudinal magnetic field, (B) transversal magnetic field.

4. Conclusions

- Magnetorheological suspensions based on mineral oil, iron and graphite micro-particles have been obtained by means of the device presented in Fig. 1 through thermal decomposition of $Fe_2(CO)_9$:
- For $T = (573 \pm 10\%)$ K The mean dimension of magnetic particles is 0.595 μm for $T = (573 \pm 10\%)$ K at a standard deviation of 0.375 μm (Fig. 3b).
- The magnetic particles obtained in mineral oil and in inert gas atmosphere (Ar) are not oxidated (Fig. 3c). They do not get oxidated with time because the oil and stearic acid layer get adsorbed on the surface of the iron micro-particles.
- The magnetization curve of MRS is of the same shape as the one of the EMRS magnetization. But, because of the graphite, the saturation level of EMRS is 7%—smaller as compared with the saturation magnetization of EMRS (Fig. 5).
- Both MRS and EMRS are non-Newtonian fluids. Their dynamic viscosity and shear stress are considerably modified under the influence of the magnetic field (Fig. 6).
- The device in Fig. 7 helps to determine the conductivity σ of the suspensions in parallel and longitudinal magnetic fields.
- MRS is not conductive. On the contrary, EMRS, due to its graphite content is conductive

owing to the pressure of the magnetic field strength.

- The electrical conductivity of EMRS, determined by means of the device in Fig. 7, comes up during time (Fig. 12), and depends on the intensity of the magnetic field as well as the field direction.

Acknowledgements

I am thankful to. E. Papp, A. Ercuta and C.T. Cheveresan from the West University of Timisoara for interesting discussions. I also like to thank O. Marinica from the Romanian Academy-Timisoara, for help in perfuming magnetorheological measurements.

References

[1] Cl. Korman, H.M. Leun, H.J. Richter, Int. J. Mod. Phys. B 10 (23–24) (1996) 3167.
[2] A.J. Margida, K.D. Weiss, J.D. Carlson, Int. J. Mod. Phys. B 10 (23–24) (1996) 3335.
[3] I. Bica, Mater. Sci. Eng. B 98 (2) (2003) 89.
[4] K. Koyama, Int. J. Mod. Phys B 10 (23–24) (1996) 3067.
[5] G.A. Flores, M.L. Ivey, J. Liu, M. Mohebi, N. Jamashi, Int. J. Mod. Phys. B 10 (23–24) (1996) 3283.
[6] P. Carletto, G. Bossis, A. Cebers, in: Proceedings of the eighth International Conference ERF and MRS, 2001, pp. 331–337.
[7] E.M. Furst, A.P. Gast, Physical Review E 61 (6) (2000) 6732.
[8] W.A. Bullough, R.J. Atkin, S. Urang, T.G. Kum, C. Mush, T. Rober, in: Proceedings of the seventh International Conference ERF and MRS, 1999, pp. 202–214.
[9] S. Melle, M.A. Rubio, G.G. Fuler, in: Proceedings of the seventh International Conference ERF and MRS, 1999, pp. 205–223.
[10] G.L. Gulley, R. Tao, in: Proceedings of the seventh International Conference ERF and MRS, 1999, pp. 331–338.
[11] K. Minagawa, T. Watanabe, M. Munakata, K. Koyama, J. Non-Newtonian Fluid Mech. 52 (1994) 59.
[12] X. Wang, F. Gordaninejad, in: Proceedings of the seventh International Conference ERF and MRS, 1999, pp. 568–578.
[13] D.-Y. Lee, N.M. Wereley, in: Proceedings of the seventh International Conference ERF and MRS, 1999, pp. 579–586.
[14] W. Kordonski, S. Gorodkin, N. Zhuravski, in: Proceedings of the seventh International Conference ERF and MRS, 1999, pp. 661–620.
[15] W.I. Kordonsky, J. Magn. Magn. Mater. 122 (1993) 395.
[16] K. Worden, W.A. Bullough, J. Haywood, Smart Technologies, World Scientific, Singapore, 2003 pp. 193–220.
[17] Y. Lee, D. Leon, in: Proceedings of the eighth International Conference ERF and MRS, 2001, pp. 70–76.
[18] M. H. Nam, Y. M. Han, S. S. Han, H. G. Lee, S. B. Choi. C. C. Cheong, in: Proceedings of the eighth International Conference ERF and MRS, 2001, pp. 302–308.
[19] H. Gavin, J. Hohagg, M. Dobossy, in: Proceedings of US-Japan Workshop on Smart Structures for Improved Seismic performance in Urban Regions, 2001, pp. 225–236.
[20] I. Bica, J. Magn. Magn. Mater. 241 (2002) 107.
[21] B. Erkus, M. Abé, Y. Fujino, Eng. Struct. 24 (2002) 281.
[22] A. Milechi, Int. J. Machine Tools Manuf. 41 (2001) 379.
[23] J. David Carlson, M.R. Jolly, Mechatronics 10 (2000) 555.
[24] D.G. Breese, F. Gordaninejad, Int. J. Vehicle Design 33 (2003) 128.
[25] I. Bica, J. Magn. Magn. Mater. 270 (2004) 321.
[26] G.A. Flores, J. Liu, in: Proceedings of the eighth International Conference ERF and MRS, 2001, pp. 146–152.
[27] St. Bednarek, J. Magn. Magn. Mater. 202 (1999) 574.
[28] J. Florea, T. Petrovici, D. Robescu, D. Stamatoiu, Poliphasic Fluids Dinamic and Their Technical Applications, Technical Press, Bucharest, 1987 (in Romanian).
[29] S. Melle, Doctoral Thesis, Ciudad Universitaria, Madrid, 2002, p. 29.